Andrzej WAINDOK[1], Paweł PIEKIELNY[1]

Opole University of Technology, Department of Industrial Electrical Engineering (1)

Transient Analysis of a Railgun with Iron Core

Abstract. *A calculation and measurement results of transients for an iron-core electrodynamic launcher have been presented in the paper. The magnetostatic field calculations have been made with using the Maxwell-ANSYS software, while the circuit part of the mathematical model has been implemented in MATLAB/Simulink package. The measurement verification has been carried out with using the original laboratory stand. The transients of excitation current, capacitor voltage and projectile velocity have been compared. A good conformity between calculation and measurement results has been obtained.*

Streszczenie. *W pracy przedstawiono wyniki obliczeń i pomiarów sygnałów zmiennych w czasie dla wyrzutni elektrodynamicznej z rdzeniem ferromagnetycznym. Do obliczeń pola magnetostatycznego wykorzystano program Maxwell-ANSYS, natomiast część obwodową modelu matematycznego zaimplementowano w pakiecie MATLAB/Simulink. Porównano ze sobą przebiegi prądu wzbudzenia, napięcia na kondensatorach oraz prędkości wylotowej elementu ruchomego (pocisku). W obliczeniach dodatkowo wyznaczono siłę działającą na pocisk oraz jego przyspieszenie. (**Analiza dynamiki akceleratora szynowego z rdzeniem ferromagnetycznym**).*

Keywords: electrodynamic accelerator, field – circuit model, transient calculation, measurement verification.
Słowa kluczowe: akcelerator elektrodynamiczny, model polowo – obwodowy, obliczenia czasowe, weryfikacja pomiarowa.

Introduction

Electrodynamic accelerators (EA), commonly called railguns, are investigated for many years [1, 2]. The first applications were a military ones [3, 4]. However, in some publication, the railguns are considered as the acceleration system for space launchers [5, 6]. In recent years, there are some research, which deals with the implementation of electrodynamic accelerators in fatigue testing of materials [7, 8]. The construction presented in the paper, should be in future used in this kind of application.

The main advantage of the railgun is the possibility to reach relatively high values of projectile energy, comparing to coilguns [9, 10, 11] - the energy obtained in military applications is about 9 MJ [12]. However, there are many important problems related to the EA work. The main is the necessity to supply the circuit with a very high current peak of kA to even MA in some milliseconds. The other problem is erosion of rails and projectile, which occurs not only during the accelerator work. The efficiency of the device is low, as well.

In order to improve parameters of railguns many different ways are chosen. First is the modification and optimization of construction [13]. Second one is optimization of supply circuit [14]. In both cases a good calculation model is needed. It could be used, for example, for thrust increasing, without the input energy increasing, which means the improvement of system efficiency.

In the presented case a field-circuit model of an electrodynamic accelerator with iron core (ICR – iron core railgun) has been created. For magnetic field analysis a 3D finite element software has been used i.e. Ansys/Maxwell [15]. The parameters obtained in the field calculations have been used in the transient (circuit) model, which has been implemented in MATLAB/Simulink software. The magnetostatic model allows to optimize the construction of the accelerator in terms of maximizing thrust. The transient model enables the analysis of supply parameters and initial conditions influence on the discharge waves, which allows to improve the efficiency of the whole system.

The calculations were verified on the original laboratory stand. The investigated ICR was developed in the Department of Industrial Electrical Engineering at Opole University of Technology.

Physical model

The picture of the accelerator with ferromagnetic core is presented in Fig. 1a. The iron core has been used in order to focus the magnetic field lines in the projectile area. Therefore, the use of the iron core contributes to increasing thrust with lower excitation current. In Fig. 1b the dimensions of the ICR are presented.
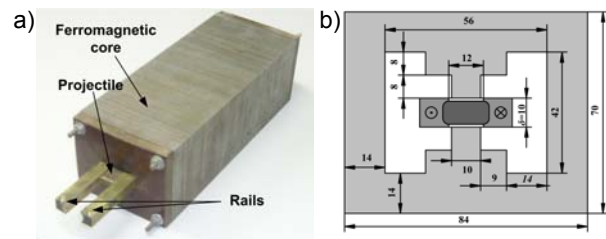
Fig.1. Electrodynamic accelerator with ferromagnetic core (ICR), (a) picture of the prototype, (b) cross-section (dimensions in mm)

In Fig. 2 the measured B/H curve of the ferromagnetic material used for the iron-core is presented. The highest value of the relative magnetic permeability is μ_r=455. This curve has been used in the magnetostatic model of the ICR.
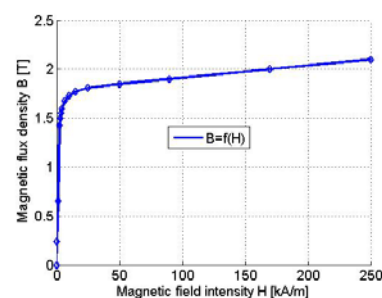
Fig.2. Measured B/H curve of the used ferromagnetic core

Fig.3. Picture of the projectile

The projectile core of 25 mm length (Fig. 3) has been made of PF CC 201 material (textolite). The active part of the projectile is made of a copper wire pulled through the

core, which ensures a good electric contact between rails and the projectile. The OFC (Oxygen-Free Copper) wire was selected, because of its high conductivity and friction resistivity, which is very important in dynamic systems with high current values. The rails have been made of brass.

The laboratory stand is presented in Fig. 4. It consists of two main parts: the power supply and measuring system. A capacitors bank with a total capacity of 133 mF and nominal voltage of 250 V was used as an energy source. To trigger shots a high power thyristor was used (model T95-1900 from Kubara LAMINA Company).
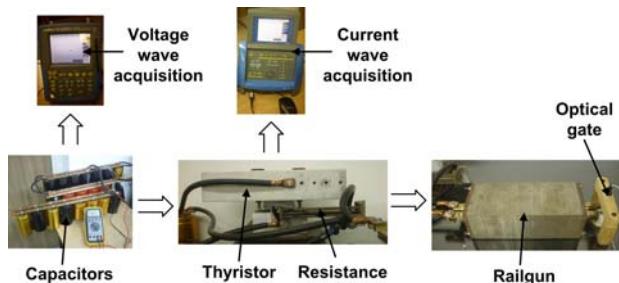
Fig.4. Laboratory stand

During the shot the following signals were recorded using an oscilloscope i.e. the voltage on the capacitor bank u, the excitation current i and the muzzle velocity of the projectile v. The voltage was measured directly. The current was measured by recording the voltage drop on the 0.517 mOhm resistance. Velocity of the projectile was calculated by measuring the time of flight through the optical gate.

Calculation model

The field-circuit calculation model consist of two parts: magnetostatic one and circuit (transient) one. The magnetic field distribution was calculated by finite element method implemented in Maxwell software. Two types of boundary conditions have been used: the voltage boundary condition on the rails ends (Fig. 5) and zero Dirichlet condition on the outer boundaries of the model. The eddy current effect has been neglected. Using this model, the chosen physical quantities of the accelerator have been determined. The current density distribution $\mathbf{J}$ was calculated with using the expression:

(1) $\mathbf{J} = -\sigma \nabla V$

where: σ – electric conductivity, V – electric potential.

The magnetic flux Φ passing through a surface S (limited by the rails and projectile, parallel to the plane X, Fig. 5a) was calculated with using the expression:

(2) $\Phi = \int_S \mathbf{B} \bullet \mathbf{n} dS$

where: $\mathbf{B}$ – magnetic flux density vector, $\mathbf{n}$ – unit vector normal to surface S.

Lorentz force $\mathbf{F}$ acting on the projectile was calculated according to the equation:

(3) $\mathbf{F} = \int_\Omega (\mathbf{J} \times \mathbf{B}) d\Omega$

where: $\mathbf{J}$ – current density vector in the projectile, Ω – volume of the projectile.

The dynamic inductance L_d of the accelerator was determined by the expression:

(4) $L_d = \dfrac{\partial \Phi}{\partial i}$

where: i – current flowing through the rails.
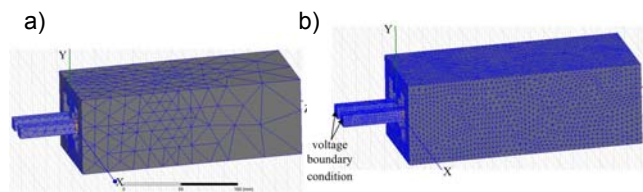
Fig.5. Two analysed discretization meshes: (a) coarse mesh, (b) dense mesh

In order to select the proper mesh discretization, calculations for two different meshes have been made (Fig. 5). In the first case the adaptive method for mesh generation has been used. The algorithm has created quite coarse mesh presented in Fig. 5a. In the second case, the maximum size of the mesh elements in each sub-area has been forced (Fig. 5b), which significantly increased the number of elements (dense mesh). In table 1 the calculation results for both types of mesh has been given. Due to small differences between obtained results (below 1%) and due to significantly shorter calculation time, the coarse mesh generated by an adaptive method, has been used. The calculation time is a very important parameter, since the calculations of integral quantities (magnetic flux, force and inductance) are made for different positions of the bullet and different excitation voltage values.

Table 1. Comparison of the calculation results for two different meshes for U_c = 200 V

Mesh type	Excitation current	Force	Calculation time	Number of elements
-	I [A]	F [N]	t [h:m:s]	n
Dense	34 333	822	4:38:18	511 306
Coarse	34 177	821	0:04:11	45 360

For transient analysis of the accelerator the circuit model has been created. Equations describing the dynamic model of the railgun have been obtained with using the Euler-Lagrange method:

(5) $\dfrac{dv}{dt} = \dfrac{F(i,x) - Dv - D_{air}v^2}{m}$; $\dfrac{dx}{dt} = v$

(6) $\dfrac{di}{dt} = \dfrac{-Ri - \dfrac{d}{dx}(\Phi(i,x))v - \dfrac{q}{C}}{\dfrac{d}{di}\Phi(i,x)}$

where: x – projectile position, v – projectile velocity, m – projectile mass, D – kinetic friction coefficient, D_{air} – air friction coefficient, R – circuit resistance, q – charge, i – excitation current, C – capacitance.

The equations (5) describe the mechanical part of the system, while the eq. (6) describes the electrical part. The above equations have been implemented in the MATLAB–Simulink software. The values of force and magnetic flux vs. projectile position x and excitation current i values ($F(i,x)$, $\Phi(i,x)$), obtained from magnetostatic model, have been included in the circuit model using a Look-up tables.

Magnetostatic calculation results

The static calculations were made for many different voltage values: from 0 to 200 V. In Fig. 6a an exemplary

distribution of the current density for U_c=200 V has been shown (the projectile is placed in the middle of the rail length). The largest value of the current density is observed on the inner edge of the projectile (approx. 3.16 kA/mm^2). The magnetic flux density distribution is nonhomogeneous in the projectile area - the highest value is observed on the supplied side and in case of U_c=200 V excitation it reaches about 5.13 T.
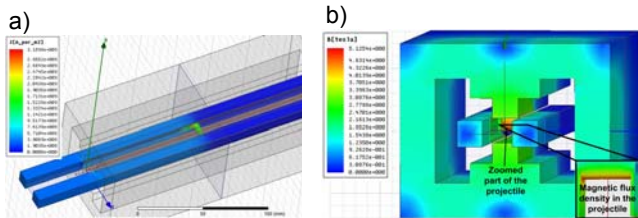
Fig.6. Calculation results for U_c=200 V: (a) the current density distribution in the rails and projectile, (b) magnetic flux density distribution
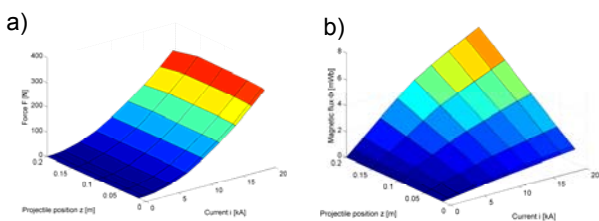
Fig.7. Calculations of the integral quantities vs. projectile position and excitation current value: (a) electrodynamic force, (b) magnetic flux
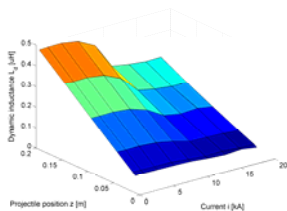
Fig.8. Dynamic inductance vs. current value and projectile position

With using the magnetostatic model, calculations of electrodynamic force, magnetic flux and dynamic inductance vs. excitation current value I and projectile position z has been carried out (Figs. 7 and 8). These parameters are very important in the proper calculation of transients (Eqs. 5 and 6). The force value varies very slightly vs. projectile position and increases exponentially vs. excitation current value (Fig. 7a). There is observed a linear increasing of magnetic flux and dynamic inductance vs. projectile position z (Figs. 7b and 8). The increasing of excitation current I below 10 kA, increases the magnetic flux linearly and only slightly affects the dynamic inductance value. For higher current values, the saturation effect is observed. It is especially visible in the case of dynamic inductance value, which decreases about 35% for I>10 kA.

Measurement verification of calculation results

In the first step the repeatability of the shots has been examined. The voltage and current waveforms for the same supply parameters and projectile position have been compared (Fig. 9). There are observed only very small differences in the recorded waveforms. It means, that these parameters depend almost only on the configuration of the system (railgun, supply system, thyristor, connection wires).
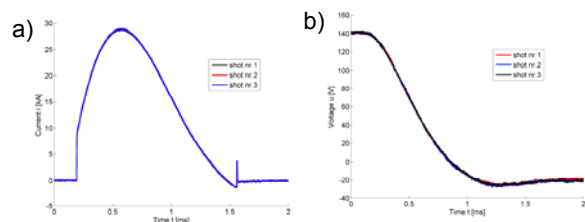
Fig.9. Repeatability tests for U_c=141 V and C=133 mF: (a) current excitation waves; (b) voltage waves

In the second step measurements for different capacity and voltage values have been made. Some results are presented in Fig. 10. The discharge time increases linearly vs. capacitance (Fig. 10a). The current peak value increases only slightly vs. capacitance and approximately linear vs. voltage value (Fig. 10). The discharge time does not depends on the voltage value (Fig. 10b).
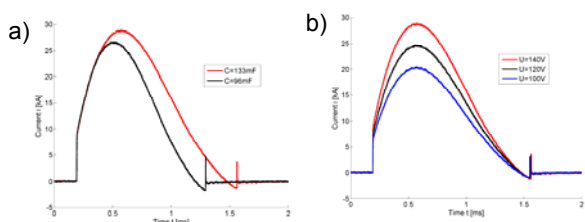
Fig.10. Current excitation waves for different supply parameters: (a) constant voltage value (U_c=141 V) - different capacity values; (b) constant capacitance value (C=133 mF) - variable voltage values

After testing the laboratory stand, the field-circuit model has been verified experimentally. The following parameters of the system have been assumed: the resistance of supply cables R=2.5 mOhm, the inductance L=0.92 µH, mass of the projectile m=4.5 g, kinetic friction coefficient D=0.2 Ns/m, air resistance coefficient C_x=1.05. The last parameter has been used in the determination of air friction coefficient. The simple expression has been used [16]:

$$(7) \qquad D_{air} = 0.5C_x gA$$

where: g – air density (1.2 kg/m^3), A – the front surface area of the projectile (97.5 mm^2).

Experiments have shown, that in the system some time lags are existing between the thyristor time triggering and the response time of the circuit rails-projectile. The system behaves in some way like a transmission line. Therefore, in the mathematical model, a fixed time delay for the inductance value has been added. The delay time has been chosen based on the experimental tests as Δt=6.6 µs. After this time, the static inductance value of the accelerator circuit steps from 0 to 0.92 µH.

In Fig. 11 results for current and voltage wave for U_c=141 V and C=133 mF have been presented. A very good conformity between calculation and measurement results is observed in case of current waves (Fig. 11a). Measured and calculated voltage waves on the capacitor bank differ only slightly (Fig. 11b). Thus, the mathematical model could be used in future theoretical investigations. There is a negative value of the capacitor voltage observed in Fig. 11b. It is due to the finite switching-off time of the thyristor (about 10 µs). In table 2 the measurement verification results of the projectile velocity for different supply conditions have been given. A very good conformity between calculations and measurements is observed. The

differences do not exceed 6%. The 40% increasing of the initial capacitor voltage, increases the velocity by 90%, i.e. the projectile energy increases by 3.7 times. The 40% increasing of capacitance, increases the projectile velocity by 45%, i.e. its energy increases by 2.1 times.
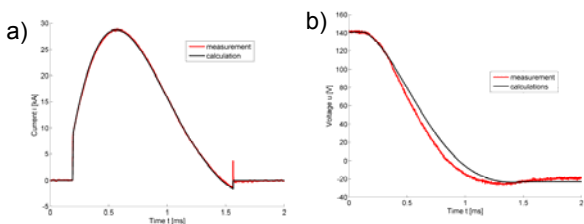
Fig.11. Measurement verification of the field-circuit model for U_c=141 V and C=133 mF: (a) excitation current wave; (b) voltage wave

Table 2. Projectile velocity for different power supply configurations

Initial capacitor voltage	Capacity	Calculated velocity	Measured velocity	Efficiency
U_c [V]	C [mF]	v [m/s]	v [m/s]	η [%]
141	133	69.03	69.44	0.82
141	96	48.25	47.89	0.54
101	133	35.94	36.55	0.44
101	96	23.23	24.75	0.28
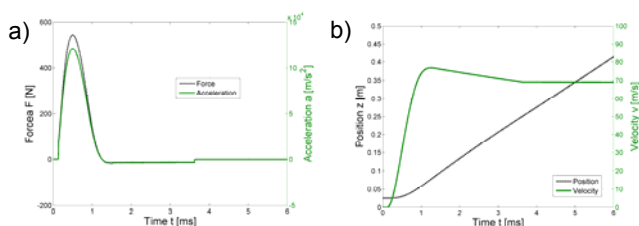
Fig.12. Calculated waves for U_c=141 V and C=133 mF: (a) force and acceleration; (b) position and velocity

Some additional calculations have been made with using the developed mathematical model. They concern quantities, which are very difficult to measure: thrust, acceleration, velocity and position of the projectile. In Fig. 12 some results for U_c=141 V and C=133 mF are presented. The start position of the projectile was on the rails beginning. The shape of the force wave is similar to the shape of the acceleration one (Fig. 12a). Due to small mass of the projectile and due to relatively high force (peak value of 545.83 N), the acceleration reaches 12130 g m/s2. The projectile accelerates during 1 ms and moves along rails during 3.4 ms (Fig. 12b). So, during 2.4 ms the projectile moves in rails without any supplying. The result is decreasing of the velocity from 77 m/s to 69 m/s. It means, that the capacitance should be increased in order to use the full potential of the accelerator.

Conclusions

Investigations of mathematical and physical models of the electrodynamic accelerator, which have been presented in the paper, lead to following conclusions:
- The capacitance influences mostly the discharge time and only slightly the current peak value (Fig. 10a).
- The initial capacitor voltage influences only the current peak value (Fig. 10b).

- The efficiency of the railgun increases along with the input energy. However, more effective is the increasing of initial capacitor voltage (Table 2).
- The friction coefficient value should be assumed very carefully – it influences considerably calculation results.

The railgun is characterized by quite complex physical phenomena. Thus, some more investigations, according both mathematical and physical models, will be carried out in future.

Autorzy: dr hab. inż. Andrzej Waindok, Politechnika Opolska, Katedra Elektrotechniki Przemysłowej, ul. Proszkowska 76, 45-758 Opole, E-mail: *a.waindok@po.opole.pl*; mgr inż. Paweł Piekielny, Katedra Elektrotechniki Przemysłowej, Politechnika Opolska, ul. Proszkowska 76, 45-758 Opole, E-mail: *p.piekielny@po.opole.pl*

REFERENCES
[1] Sink D.A., Krzastek L.J., Design and modeling considerations for experimental railgun armatures, *IEEE Trans. Magn.,* 27 (1991), n.1, 266-271.
[2] Katsuki S., Akiyama H., Eguchi N., Sueda T., et. al., Behaviors of plasma armature in the augmented railgun using a permanent magnet*, IEEE Trans. Magn.*, 31 (1995), n.1, 183-188.
[3] Jamison U.A., Burden H.S., Measurements of plasma properties from a large bore, plasma armature railgun, *IEEE Trans. Magn.*, 25 (1989), n.1, 256-261.
[4] Hundertmark S., Schneider M., Simicic D., Vincent G., Experiments to increase the used energy with the PEGASUS railgun, *IEEE Trans. on Plasma Science*, 42 (2014), n.10, 3180-3185.
[5] McNab I.R., Progress on hypervelocity railgun research for launch to space, *IEEE Trans. Magn.*, 45 (2009), n.1, 381-388.
[6] Lehmann P., Reck B., Vo M.D., Behrens J., Acceleration of a suborbital payload using an electromagnetic railgun, *IEEE Trans. Magn.*, 43 (2007), n.1, 480-485.
[7] Poniaev S., Bobashev S., et. al., Small-size railgun of mm-size solid bodies for hypervelocity material testing, *Acta Astronautica,* 109 (2015), 162-165.
[8] Hogan J.D., Spray J.G., et. al., Dynamic fragmentation of planetary materials: ejecta length quantification and semi-analytical modelling, *International Journal of Impact Engineering,* 62 (2013), 219–228.
[9] Mikołajewicz J., Analiza stanów pracy kaskadowej wyrzutni elektromagnetycznej na podstawie polowego modelu zjawisk, *Przegląd Elektrotechniczny*, 82 (2006), nr.12, 20-23.
[10] Waindok A., Mazur G., Mutual inductances in a mathematical model of the three-stage reluctance accelerator, *Proceedings of the IIIrd International Students Conference on Electrodynamics and Mechatronics (SCE III),* Opole, Poland, October 6-8, 2011, 115-118.
[11] Domian J., Kluszczyński K., Hybrid pneumatic-electromagnetic launcher – general concept, mathematical model and results of simulation, *Przegląd Elektrotechniczny*, 89 (2013), n.12, 21-25.
[12] O'Rourke R., Navy lasers, railgun and hypervelocity projectile: background and issues for congress, *Congressional Research Service*, June 17, 2016.
[13] Waindok A., Piekielny P., Analysis of selected constructions of the electrodynamic accelerator, *International Symposium on Electrodynamic and Mechatronic Systems (SELM),* Zawiercie, Poland, May 15-18, 2013, 51-52.
[14] Piekielny P., The Influence of supply circuit modification on electrodynamic accelerator parameters, *Zeszyty Naukowe Politechniki Opolskiej,* 72 (2016), 63-64.
[15] Kohnke P., ANSYS Mechanical APDL Theory Reference, November 2013.
[16] Stöcker H., Nowoczesne kompendium fizyki, PWN, Warszawa, 2010.